TRANSPORT PHENOMENA DURING SOLIDIFICATION OF A VERTICAL CASTING OF STEEL: A MULTIPHASE NUMERICAL STUDY

Y. Zheng[1], M. Wu[1,2*], A. Kharicha[1,2], A. Ludwig[1]

[1] Chair of Modeling and Simulation of Metallurgical Processes, Montanuniversitaet Leoben, Austria
[2] Christian Doppler Lab for Advanced Simulation of Solidification and Melting, Montanuniversitaet Leoben, Austria
[*] Corresponding author: menghuai.wu@unileoben.ac.at

ABSTRACT: A three-phase mixed columnar-equiaxed solidification model considering fluid flow, heat and solute transport is applied to simulate the solidification in a vertical continuous casting. The key features of solidification phenomena in this process, such as evolution of columnar phase, evolution and floatation/sedimentation of equiaxed crystals, thermal solutal convection of the melt and the flow caused by crystal sedimentation, development of as-cast structure, the columnar-to-equiaxed transition (CET), and formation of macrosegregation, are simulated. It is predicted that there is an equiaxed zone in the central part of the strand, and the rest section is filled with columnar phase (or dominant with columnar phase). A relatively strong negative segregation in the equiaxed zone and a mostly neutral concentration in the columnar region are found. Near the CET, there is a so-called middle radius positive segregation band. Formation mechanisms of this segregation pattern are discussed.

KEYWORDS

columnar-equiaxed solidification, large vertical continuous casting, macrosegregation.

INTRODUCTION

Vertical continuous casting technique is recently applied to produce large round steel strands and to replace some of the conventional ingot castings [1-3]. As shown in Fig. 1 (a), the molten steel is conducted into the mold through a submerged entry nozzle (SEN) and the melt solidifies against the water-cooled copper mold. Below the copper mold, water and air mist sprays cool the strand continuously to maintain solidification of the melt core until it becomes fully solid. One problem is that the as-cast product is prone to macrosegregation, when the diameter of the strand increases. A special segregation profile across the section is developed, which differs from those of conventional continuously cast round products (small diameter) and conventional strands. No experience can be referred to control the macrosegregation, and experimental investigation would be extremely costly. Therefore, a numerical study of the flow phenomena and the formation mechanisms of macrosegregation during solidification is performed. In present paper, a three phase mixed columnar-equiaxed solidification model by Wu [4] is applied to analyze flow, solidification, columnar equiaxed phase transfer and evolution of macrosegregation in the vertical continuous casting. The aim of this paper is to simulate the as-cast structure including macrosegregation.

1. NUMERICAL MODEL

A volume averaged Eulerian-Eulerian three phase mixed columnar-equiaxed solidification model is applied. Detailed descriptions of the model can be found in previous studies [4-7]. In the following a brief description and further simplifications of the numerical model are given:

a) Three phases are considered: primary liquid melt (ℓ), equiaxed phase (e), columnar phase (c). Ideal crystal morphologies are assumed: spheres for equiaxed (globular) grains, and cylinders for columnar (cellular) dendrite trunks.
b) Both liquid and equiaxed phases are moving phases for which the corresponding velocity

INDEX

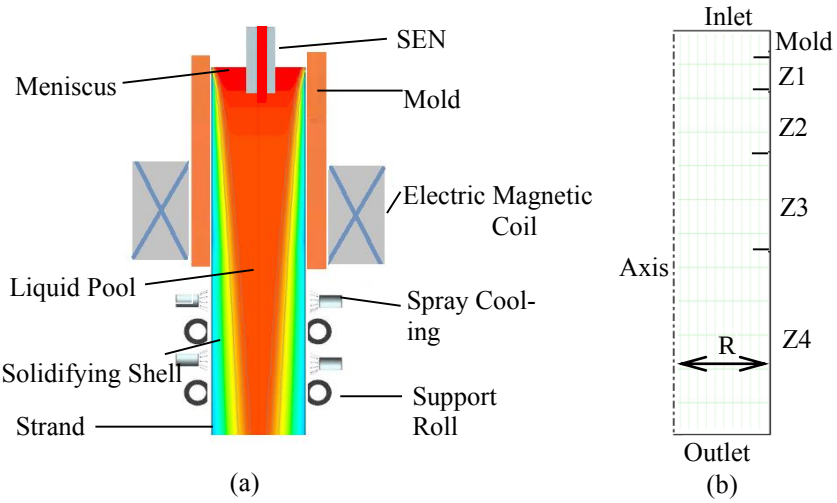

Fig. 1. Schematic of vertical steel continuous casting process (a) and the calculation domain in 2D axial symmetry (b).

fields ($\vec{u}_\ell$) and ($\vec{u}_e$) are solved. The motion of columnar phase is set equal to the casting ($\vec{u}_{pull}$).

c) Enthalpy equations for all 3 phases are solved. A large inter-phase volume heat transfer coefficient between the phases is applied to balance the temperatures among the phases. Therefore only one temperature field is necessarily used to represent all three phases.

d) Volume-averaged concentrations for each phases (c_ℓ, c_e, c_c) are solved by global species conservation equations. To evaluate macrosegregation, a mixture concentration is defined

$$c_{mix} = \frac{c_\ell \rho_\ell f_\ell + c_e \rho_e f_e + c_c \rho_c f_c}{\rho_\ell f_\ell + \rho_e f_e + \rho_c f_c} \quad (1)$$

or it is sometimes evaluated with a so-called macrosegregation index:

$$\Gamma = 100 \frac{c_{mix} - c_0}{c_0} \quad (2)$$

e) A constant number density (n_e) of equiaxed crystals, predefined to mimic the origin of crystals by electro-magnetic stirring, is assumed to enter the domain from the inlet.

f) Growth of equiaxed crystals and columnar crystals are explicitly calculated according to diffusion-governed growth kinetics. Interactions between equiaxed crystals and columnar crystals are considered. Therefore, the columnar-to-equiaxed transition (CET) can be predicted.

g) No shrinkage porosity is considered. The Boussinesq approach is employed to model thermo-solutal convection, grain sedimentation, and sedimentation-induced melt convection.

Due to the axis symmetry, the calculation domain is set up in Fig. 1(b). The influence of the submerged entry nozzle (SEN) is ignored and the electromagnetic force is not taken into account. The liquid melt with superheat is assumed to be conducted into the mold continuously from the meniscus with constant velocity, and to be cooled down by the primary cooling (mold) and second cooling zone (from Z1 to Z4). Gravity acts in the axial direction. The model domain is discretized by a mesh of 20×40 mm^2. The physical properties and boundary parameters are listed in Tab. 1.

The model is realized numerically with a control-volume based finite difference method through the ANSYS FLUENT software version 14.5, run on a Cluster paralleled with 12 cores. Both the liquid and solid share a single pressure field *p*. The pressure correction equation is obtained from the sum of the normalized mass continuity equations using an extended SIMPLE algorithm [8]. Transient calculations were performed in order to estimate steady-state. For each time step, 60 iterations were adopted to decrease the normalized residual of concentration, flow quantities and pressure below 10^{-4} and enthalpy below 10^{-6}. It took about 15 days for a single simulation.

INDEX

2. SIMULATION RESULTS

The results analyzed below include distributions of the temperature (T), liquid volume fraction (f_ℓ), equiaxed volume fraction (f_e), columnar volume fraction (f_c), velocity of liquid melt ($\vec{u}_\ell$) and velocity of equiaxed crystals ($\vec{u}_e$) and macrosegregation index (Γ). Here only the steady-state results are evaluated.

Tab. 1. Simulation settings and material properties.

Contents		Value
Steel composition (wt.% C)		0.432
Latent heat (J/kg)		2.71×10^{5}
Heat conductivity (W/m/K)		34.0
Specific heat (J/kg/K)		500.0
Initial equiaxed number density (m^{-3})		1.0×10^{8}
Density (kg/m^3)		6990.0
Density diff. between liquid and equiaxed (kg/m^3)		150.0
Viscosity (kg/m/s)		4.2×10^{-3}
Strand diameter (m)		0.6
Strand length (m)		20.0
Casting speed (m/s)		3.3×10^{-3}
Pouring temperature (K)		1795.0
Mold	Mold length (m)	0.7
	Heat transfer coefficient ($W/m^2/K$)	1000.0
Z1	Length (m)	0.53
	Heat transfer coefficient ($W/m^2/K$)	333.0
Z2	Length (m)	1.52
	Heat transfer coefficient ($W/m^2/K$)	195.0
Z3	Length (m)	2.65
	Heat transfer coefficient ($W/m^2/K$)	111.0
Z4	Length (m)	14.6
	Heat transfer coefficient ($W/m^2/K$)	10.0

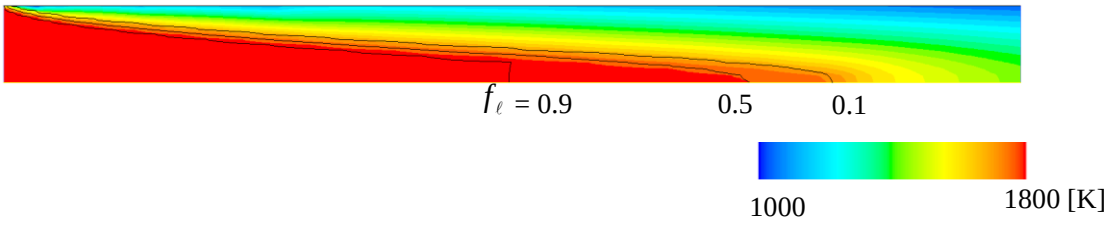

Fig. 2. Temperature distribution overlapped with the liquid volume fraction isolines (f_ℓ = 0.1, 0.5, and 0.9). All of contours are scaled by a factor of 1/4 in the longitudinal direction.

2.1 Temperature Distribution

The calculated temperature field (Fig. 2) is quite symmetrical with a relatively high temperature in the upper center of the strand due to the superheat (25K) of the steel melt, a lower temperature in the outer part of the strand because of the heat extraction on the strand surface thorough water and air-cooling. The pool depth, the so-called metallurgical length, is mainly governed by the thermal field. Cooling curves along the centerline and strand surface are plotted in Fig. 3. The cooling curve along the strand surface clearly indicates different cooling zones from those discontinuity points. The temperature along the stand surface is much lower than that along the center. No obvious change in T occurs along the axis initially from the meniscus until reaching a turning point, at which the cooling rate increases dramatically. This turning point indicates the

INDEX

end of solidification at the casting center. The positon of metallurgy length is about 16 m.

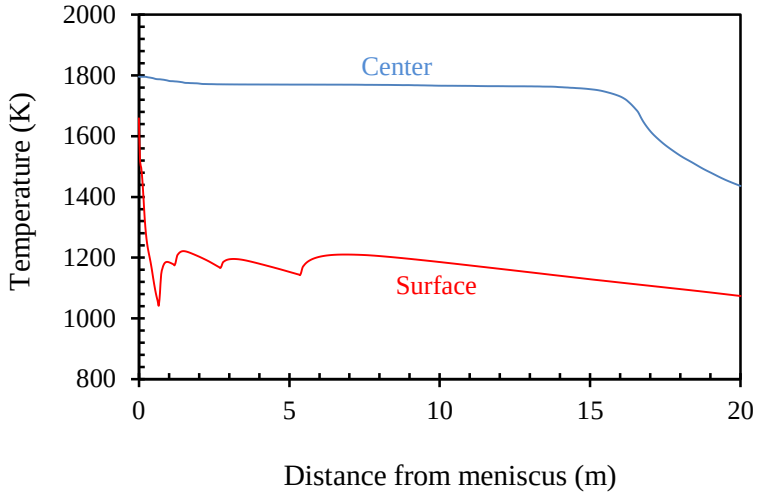

Fig. 3. Temperature profiles along centerline and casting surface.

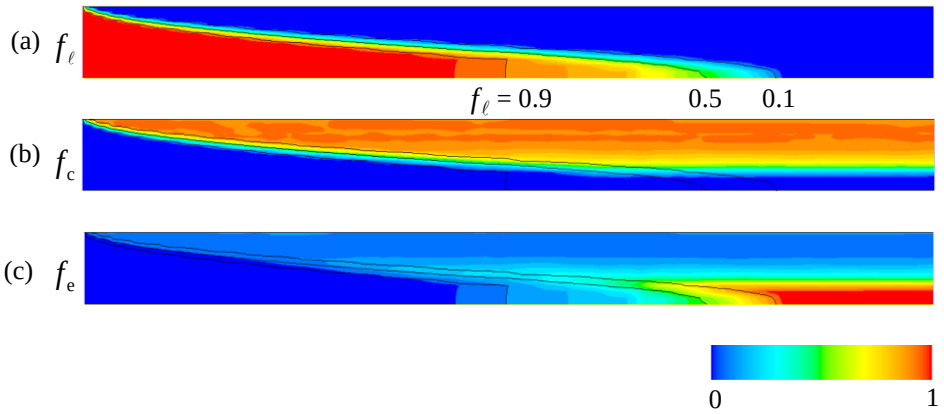

Fig. 4. Phase distributions overlapped with isolines (f_ℓ = 0.1, 0.5 and 0.9): (a) liquid volume fraction f_ℓ; (b) columnar volume fraction f_c; (c) equiaxed volume fraction f_e.

2.2 As-cast Structure and CET

The as-cast structure of the strand is described by the distributions of the three phases, which are shown in Fig. 4. The liquid phase dominates the upper center part of the domain. The rest of the domain is occupied by the two solid phases: the columnar phase in the outer part and the equiaxed phase in the center. Growth of equiaxed crystals and columnar crystals are explicitly calculated according to diffusion-governed growth kinetics. Interaction between equiaxed and columnar phase is considered. When the volume fraction of the equiaxed phase ahead of the columnar tip front is bigger than 0.49, the progress of the columnar tip front is terminated mechanically by the so-called hard block mechanism. Moreover, solutal blocking, which refers to the growth of columnar being stopped by the solute-enriched melt, is also introduced [9]. Therefore, the columnar-to-equiaxed transition (CET) is predicted.

The phase distribution along the centerline and in radial direction at the outlet are analyzed qualitatively (Fig. 5). Along the centerline, f_ℓ decreases while f_e increases, and both phases add up to 1, giving no space for the columnar

INDEX

phase, Fig. 5(a). The columnar zone is predicted in the outer radial region. If we define the position of CET (columnar-to-equiaxed transition) at f_e = 0.5, the equiaxed zone takes 37% of the strand radius. That is ca. 13% of whole casting cross section.

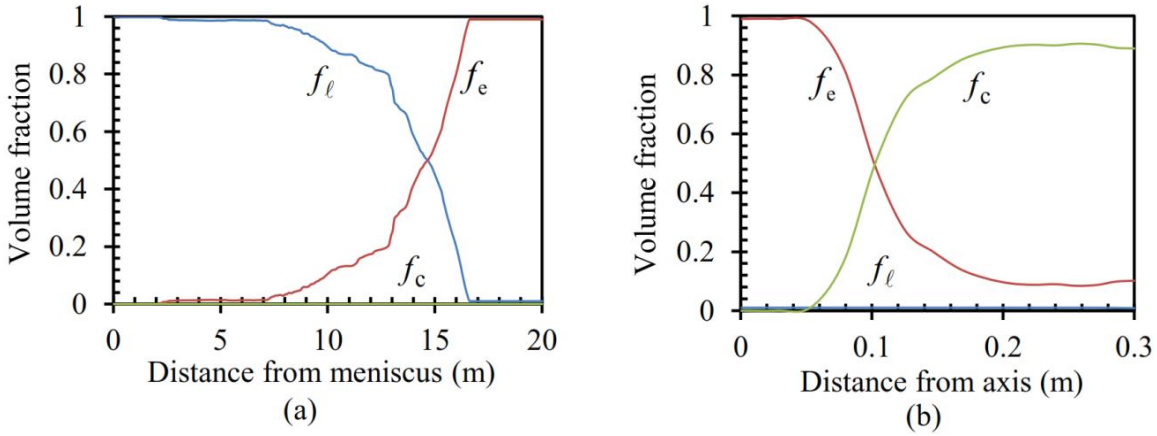

Fig. 5. Phase distributions (a) along the centerline and (b) along the radial the direction at outlet.

2.3 Macrosegregation

Fig. 6 shows the contour of the macrosegregation index, Γ. In the mold region near the meniscus, Γ is zero (neutral concentration in the original melt). In the liquid core region, where f_ℓ is still larger than 0.9, the melt has a positive value of Γ indicating the enrichment of solute elements. When f_ℓ in the casting center drops to about 0.5, strong negative segregation develops. Between the two distinguish areas is the location where velocity of the equiaxed crystals becomes equal to the casting speed (no relative velocity between equiaxed and the moving strand). The rapid development of negative segregation at the transition point corresponds to the pile-up of the equiaxed crystals due to settlement. On surface of the strand, a tiny negative segregation zone is predicted.

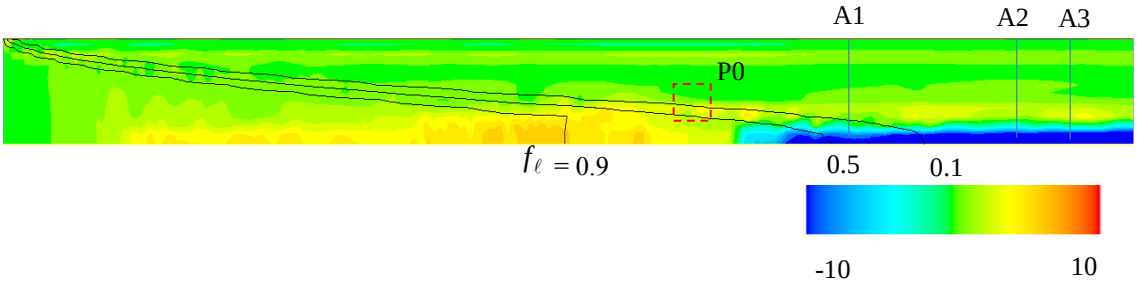

Fig. 6. Distribution of macrosegregation index Γ overlapped with liquid volume fraction isolines f_ℓ =0.1, 0.5 and 0.9.

The distribution of Γ changes dynamically, especially when f_ℓ is still larger than 0.5. However, the pattern is almost fixed when f_ℓ is smaller than 0.1. A further interesting phenomenon is that a discontinuous positive segregation zone in the middle radius region (discontinuous yellow zones, just located above the centerline blue zone) is also developing around the central negative segregation zone. We call this positive segregation band as middle-radius positive segregation.

Macrosegregation index Γ profiles along the centerline and along the radial direction at different positions are presented in Fig. 7. Along the centerline (Fig. 7(a)), Γ near the meniscus is zero indicating the initial concentration in

INDEX

the original melt. Below that Γ becomes positive and then followed by a positive-to-negative transition at about 13 m from the meniscus. The negative Γ in the casting center reaches an extreme of -13%. After the positive-to-negative transition, the Γ curve fluctuated slightly. The final segregation profiles at different strand sections are analyzed along the radial direction (A1, A2 and A3), as plotted in Fig. 7 (b). The segregation profile along the section A3 represents the final segregation profile. Near the casting surface, a slightly negative segregation is predicted. Nearby, there is a slightly positive segregation zone. The most significant segregation zones are the mid-radius positive segregation and the center negative segregation. The positive segregation index at the mid-radius region (ca. 80 mm from axis) reaches the extreme of about 3%.

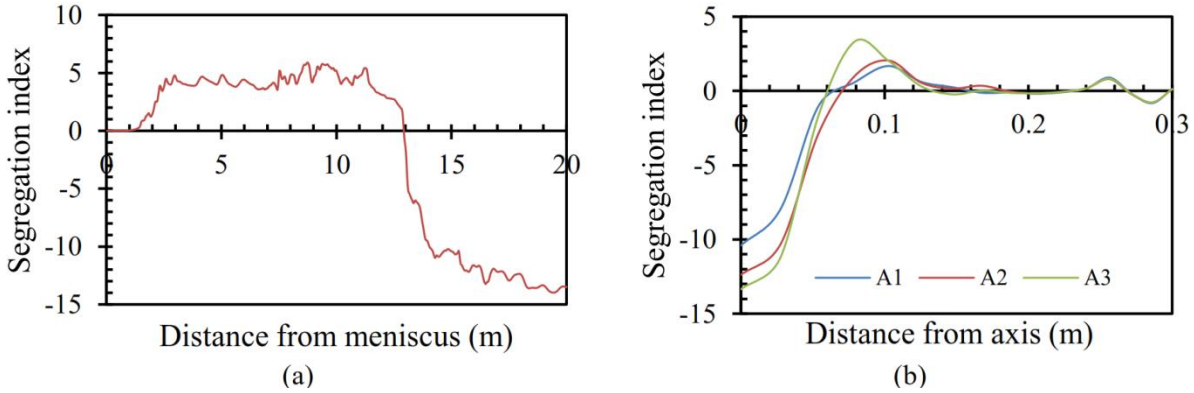

Fig. 7. Macrosegregation index profiles: (a) along the centerline and (b) along the radial direction at three different sections A1-A3 as marked in Fig. 6.

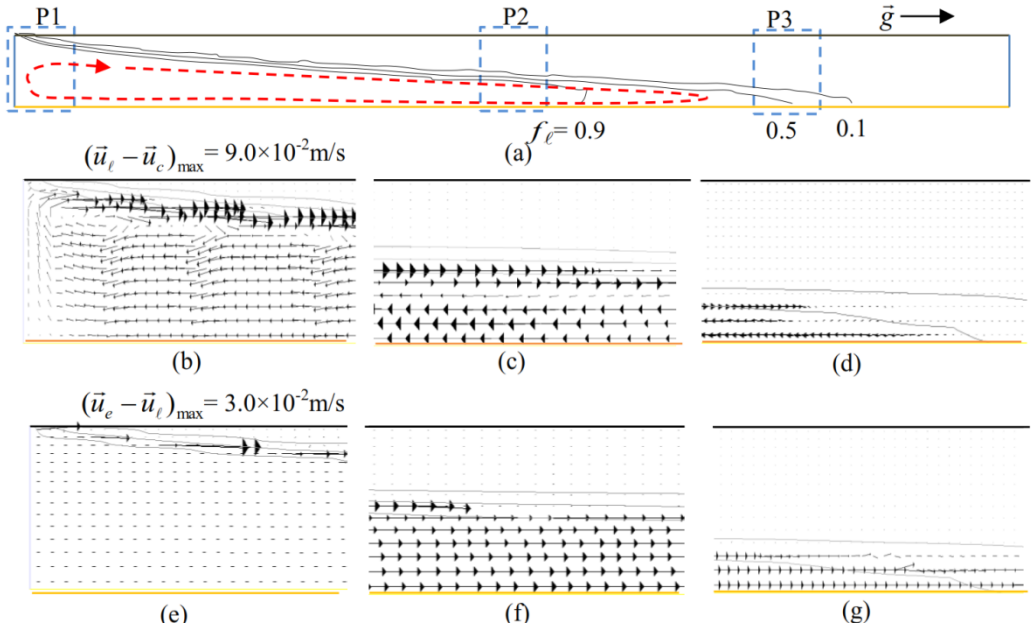

Fig. 8. Relative velocity vectors: (a) global view of the strand and schematic of the liquid flow; (b), (c) and (d) relative velocity between liquid and columnar in P1, P2, P3 Zones; (d), (e), (f) relative velocity between equiaxed and liquid in P1, P2 , P3 Zones.

INDEX

3. DISCUSSION

3.1 Macrosegregation Mechanisms

Macrosegregation occurs due to the relative movement between phases. Both thermal-solutal convection and equiaxed crystal sedimentation are dynamic and unstable. Fig. 8(a) gives a global view of the strand. Fig. 8 (b)-(d) are zoom-in views of the relative velocities between liquid and columnar phases in zones P1, P2 and P3, respectively. Similarly, Fig. 8 (e)-(f) are zoom-in views of the relative velocities between equiaxed and liquid phases in zones P1, P2 and P3. In the upper part of the strand near the mold wall, many vortexes form. In the middle of the domain, a large circulation loop occur. The melt sinks along the columnar front and rises at the casting center. At the bottom of the pool, the rising melt transports and mixes the rejected carbon solute into the liquid pool, leading to a solute enriched area in the upper part of the domain (Fig. 8 (b)-(d)). The relative equiaxed-liquid velocity is always downwards due to the density difference between liquid and equiaxed. Therefore the equiaxed phase would sediment and pile up at the bottom of the liquid pool, leading to a negative segregated center (Fig. 8 (e)-(f)).

The relative motion between phases is also responsible for other macrosegregation phenomena, such as the above-mentioned mid-radius positive macrosegregation, whose formation mechanism is demonstrated in Fig. 9. The background color fluctuation in Fig. 9(a) indicates the formation of the mid-radius positive macrosegregation (red color for positive). The black vectors show the motion of equiaxed relative to columnar crystals. The white vectors illustrate the motion of liquid melt relative to the columnar crystals. The formation mechanism for this mid-radius positive segregation is mainly due to the motion of equiaxed crystals, which tend to leave the mush zone and sediment downwards at the casting center. In the mush zone near the columnar tip front the space of the leaving equiaxed crystals (solute-depleted) is filled by the solute-enriched melt (Fig. 9(b)). This kind of relative motion causes the local increase of the mixture concentration, *i.e.* the formation of a positive macrosegregation.

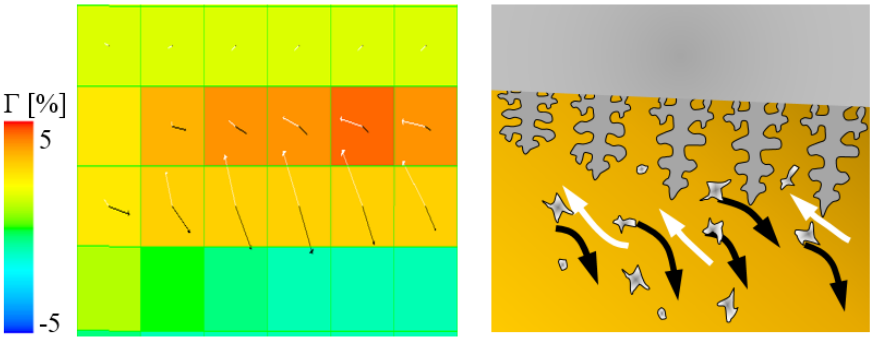

Fig. 9. Analysis of the formation mechanism of the middle-radius positive segregation: (a) zoom-in of P0 as marked in Fig. 6; (b) schematic of the relative motion between phases in a representative volume element.

3.2Evaluation of the segregation results

The three-phase mixed columnar-equiaxed solidification model used to simulate macrosegregation in a vertical continuous casting is able to successfully explain the segregation pattern from the relative motion between liquid, columnar and equiaxed phases. The predicted segregation agrees qualitatively well with the industry praxis (Primetals): central negative segregation zone surrounded by a slightly positive segregation ring. It is worth mentioning that the electromagnetic stirring (EMS) is currently not modeled explicitly. The most important function of EMS is to promote the equiaxed zone in the casting center. In the current model, the effect of EMS is considered by setting a predefined initial number density of equiaxed crystals, depending on the intensity of the EMS-induced forced convection. Here

INDEX

the initial number density of equiaxed crystals is determined by a parameter study to fulfill the condition that the calculated equiaxed zone takes around 30~40% of the strand radius (industry experience).

One may notice that different segregation patterns were observed in continuous casting [10-16]. In conventional small bloom and billet castings without EMS, the columnar crystals grow typically towards the casting center, leading to the so-called bridging and resulting in positive macrosegregation in the casting center [10, 11]. Nowadays the utilization of EMS is popular. The EMS can promote significant amount of equiaxed crystals ahead of the columnar tip front. With the increase of the equiaxed zone in the casting center, segregation pattern can change from aforementioned positive segregation to negative segregation [12-13]. Buoro *et al.* [14] reported that the ∅ 500 mm steel strand cross section had a negative segregation in the center. These references support the current modeling result.

Some other industry results show different segregation patterns, conflicting with the current modeling result. Sun *et al.* [15] reported that there is a remarkable positive macrosegregation in the center of a round steel bloom (350 mm diameter) with F-EMS. Li *et al.* [16] reported the similar results with positive macrosegregation at the center of a 380×280 mm^2 steel bloom under complex EMS condition. The major difference is that they have used F-EMS just before end of solidification, which is not considered in the current vertical casting process. The F-EMS can modify the flow pattern and the motion of the settling equiaxed crystals dramatically.

Although the first attempt to simulate macrosegregation in the large vertical continuous casting gives some promising results and helps to interpret the formation mechanisms of some segregation phenomena, the current model is still subject to further improvement. The origin of equiaxed crystals by heterogeneous nucleation and fragmentation due to the effect of EMS are not properly modeled. The flow pattern influenced by SEN in the mold is also not calculated. Full 3D simulation is needed to give a more comprehensive understanding of the transport phenomena. Additionally, quantitative experimental validation is desired.

4. SUMMERY

1) A first attempt to simulate the macrosegregation in a large vertical continuous casting (∅ 600 mm) by using a three-phase mixed columnar-equiaxed solidification model was made. The modeling results give valuable insight into the solidification process of the large vertical continuous casting.
2) The solidification process in such a large vertically cast strand includes: evolution of columnar dendrites, evolution and flotation/sedimentation of equiaxed crystals, thermal-solutal convection and flow caused by crystal drag, development of a columnar-to-equiaxed transition, and formation of macrosegregation.
3) The calculated segregation pattern agrees qualitatively with the industry praxis: negative segregation in the center equiaxed zone, surrounded by a middle-radius positive segregation ring in the CET region. The relative motion between different phases successfully explains the segregation pattern.
4) Further modeling effort, especially for the origin of equiaxed crystals by heterogeneous nucleation and fragmentation due to electromagnetic stirring, and the corresponding experimental evaluation are required in future.

ACKNOWLEDGEMENTS

The authors acknowledge the financial support from Austrian Research Promotion Agency (FFG) through the project of Bridge Early Stage (No. 842441), as well as the technical support from the industrial partner Primetals Technologies (former Siemens VAI).

REFERENCES

[1] H. Cherukuri and R. Johnson: Int. J. Mech. Sci. 43, (2001), p.1243.
[2] P. Lopez, N. Jalali, J. Björkvall, U. Sjöström and C. Nilsson: ISIJ Int. 54, (2014), p.342.

INDEX

[3] F. Wimmer, H. Thöne and P. Pennerstorfer: Metall. Res. Techn. 112, (2015), p.1.
[4] M. Wu and A. Ludwig: Metall. Mater. Trans. A 37, (2006), p.1613.
[5] M. Wu, J. Li, A. Ludwig and A. Kharicha: Comp. Mater. Sci. 92, (2014), p.267.
[6] M. Wu, J. Li, A. Ludwig and A. Kharicha: Comp. Mater. Sci. 79, (2013), p.830.
[7] J. Li, M. Wu, A. Ludwig and A. Kkaricha: Int. J. Heat Mass Trans. 72, (2014), p.668.
[8] S. V. Patankar (1980) Numerical Heat Transfer and Fluid Flow (Carlsbad: Hemisphere Pub. Corp.)
[9] A. Ludwig and M. Wu: Mater. Sci. Eng. A 413, (2005), p.109.
[10] O. Bode, K. Schwerdtfeger, H. Geck and F. Höfer: Iron and Steelm. 35, (2008), p.137.
[11] J. Moore, Iron and Steelm: 10, (1980), p.8.
[12] K. Ayata, H. Nakata, J. Miyazaki, T. Nozaki and T. Mori, Steelmaking Proceedings 68, (1985), p.463.
[13] D. Zhou, F. Jie, W. Ping, X. Junhao, X. Yaqing and L. Zheng: J. Mater. Sci. Techn. 16, (2000), p.273.
[14] S. Buoro and G. Romanelli: Iron and Steel Technology 9, (2012), p.39.
[15] H. Sun and L. Li: Ironmaking and Steelmaking (2015) D 10.1179/1743281215Y.0000000018
[16] J. Li, B. Wang, Y. Ma and J. Cui, Mater. Sci. Eng. A 425, (2006), p.201.

INDEX